

# UHECR propagation in the Galactic Magnetic Field

Serguei Vorobiov\*<sup>†</sup>, Mustafa Hussain\*, and Darko Veberič\*<sup>‡</sup>

\*Laboratory for astroparticle physics, University of Nova Gorica, Slovenia.

<sup>†</sup>Email: sergey.vorobyev@p-ng.si

<sup>‡</sup>J. Stefan Institute, Ljubljana, Slovenia

**Abstract**—Extensive simulations of the ultra-high energy cosmic ray (UHECR) propagation in the Galactic magnetic field (GMF) have been performed, and the results are presented. The use of different available models of the large-scale GMF and/or primary particle assumptions leads to distinctly different deflection patterns of the highest energy cosmic rays (CR). The lensing effects of the Galactic field modify the exposure of an UHECR experiment to the extragalactic sky. To quantify these effects for the Pierre Auger experiment, we performed a correlation analysis of the simulated cosmic ray event samples, backtracked from the Earth to the Galactic border, with the active galactic nuclei (AGN) from the 12th edition of the Véron-Cetty and Véron catalogue. Further forward-tracking studies under plausible UHECR sources scenarios are needed to allow for direct comparison with the observed correlation between the nearby AGN and the highest energy Auger events.

## I. INTRODUCTION

Magnetic fields in the Milky Way and other galaxies are investigated by means of measurements of the Faraday rotation of the polarized light from pulsars and extragalactic sources, and through detection of synchrotron radiation emitted by relativistic electrons [1], [2]. The observations of spiral galaxies like ours suggest that there is a large-scale field, that in the first approximation follows the spiral arm structure, and is parallel to the galactic disk. In the vicinity of the Sun such large-scale field is pointing approximately in direction of galactic latitude  $\ell = 80^\circ$ . The spiral field extends above and below the galactic disks on a kiloparsec scale and forms a kind of halo, which is confirmed by observations of the galaxies that are seen edge-on. A random Galactic magnetic field, of the strength similar to that of the regular component, has also been observed [1]. The coherence length of the turbulent field is at most of the order of several tens of parsecs. The average strength of the total magnetic field is about  $6 \mu\text{G}$  near the Sun, and increases towards the Galactic Center region. The observations of the Galactic diffuse soft X-rays indicate on a possible CR and gas pressure driven wind, which would transport magnetic fields from the disk to the halo [3], [4].

The observed Faraday rotation measures (RM) allow to probe the Galactic magnetic field in the Solar proximity [5], [6], [7]. However, the limited data sample makes the interpretation of these observations difficult. In addition, the RM measurements provide the line-of-sight convolution of the magnetic field with the thermal electron density, which in turn is not well known. New radio polarization observations, with better sensitivity and angular resolution are needed to obtain

more conclusive picture of the magnetic field distribution in the Milky Way. A significant improvement of the data will be provided by new-generation radio telescopes. One of such instruments, the Low Frequency Array (LOFAR), is already under construction [8]. LOFAR will be in particular able to trace the magnetic fields in halo regions of the Milky Way and other galaxies, through detection of a few meters radio synchrotron emission from low energy cosmic rays [9].

The Pierre Auger Observatory [10] provides a new and independent way of studying cosmic magnetic fields, by collecting cosmic ray events at the extreme energies (above  $10 \text{ EeV} \equiv 10^{19} \text{ eV}$ ) with unprecedented statistics and data quality. Recently, the Pierre Auger Collaboration observed [11], [12] a significant anisotropy in the arrival directions of cosmic rays above  $\simeq 60 \text{ EeV}$ . These cosmic rays correlate over angular scales less than  $6^\circ$  with the locations of nearby ( $D < 100 \text{ Mpc}$ ) AGN from the 12th edition of the Véron-Cetty and Véron (VCV) catalogue [13]. The Pierre Auger experiment has also detected [14] a strong steepening of the cosmic ray flux above  $4 \times 10^{19} \text{ eV}$ . Both observations are consistent with the standard scenarios of the UHECR production in the extragalactic astrophysical acceleration sites and thus represent the important step towards the “charged particle astronomy”.

The final way the CR astronomy will be done will strongly depend on the primary mass composition of the highest energy cosmic rays, since the magnetic deflections scale in proportion to the CR atomic number  $Z$ . The elaboration of relevant analysis methods requires detailed investigation of the UHECR propagation in cosmic magnetic fields, and first of all in the Galactic field. The different aspects of the UHECR propagation in the GMF have been extensively covered in the literature, the non-exhaustive list of previous results can be found in [15], [16], [17], [18], [19], [20], [21]. We present in this paper results of our own studies, performed in the light of the observed AGN correlation. We used the standard method of CR backtracking (see Sec. II). Three distinctive large-scale field models have been chosen (Sec. III). A large number of CR events has been simulated using energy spectrum, arrival direction distribution, and mass composition described in Sec. IV, and propagated under the assumed GMF models. Resulting magnetic deflections are presented in Sec. V. Modification of the extragalactic exposure due to the large-scale GMF lensing effects is discussed in Sec. VI, followed by conclusions.

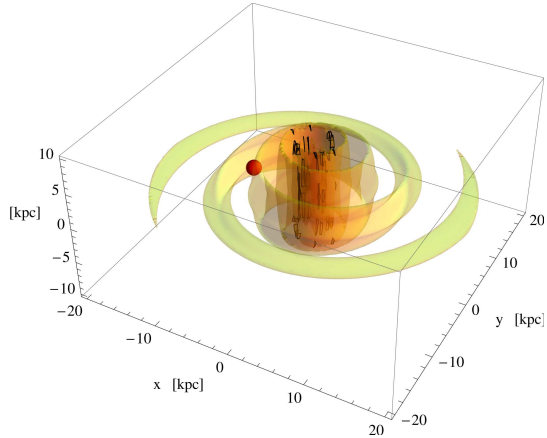


Fig. 1. The spiral disk field in the HMR models [16]. The volume of galactic region with magnitude of magnetic field larger than  $1 \mu\text{G}$  is shown in yellow-green. The position of the Solar system is denoted by a red sphere.

## II. CR BACKTRACKING IN THE GALACTIC FIELD

Since the energy loss length in the local Universe largely exceeds the size of the Galaxy (see, for example, [22], [23], [24]), we can neglect the energy losses when considering the propagation of the ultra-high energy cosmic rays through the Milky Way. This makes it possible to inverse the problem and, instead of following the trajectory of a particle from the Galactic halo border till the arrival on Earth from a certain direction, to propagate the corresponding anti-particle from Earth in the same direction (backtracking method). The trajectory of a UHE cosmic ray is then obtained by integration of the equations of motion of an ultra-relativistic particle with the energy  $E$  and charge  $q$  in a quasi-static magnetic field  $\vec{B}$ :

$$\frac{d\vec{r}}{dt} = \hat{v}, \quad \frac{d\hat{v}}{dt} = \frac{qc}{E} \hat{v} \times \vec{B}, \quad (1)$$

where  $\hat{v} = \vec{p}/|\vec{p}|$ ,  $\vec{p} = E d\vec{r}/c^2 dt$ , is the unit vector parallel to the velocity of the cosmic ray. Since in the highly structured Galactic magnetic field the field strength can vary significantly along the cosmic ray trajectory, we have implemented for the integration of the equations of motion (1) the Runge-Kutta 5<sup>th</sup> order scheme (RK5) with the adaptive step size control [25]. To avoid the “numerical dissipation” of the cosmic ray energy  $E$  (the effect studied in detail in [26]), we imposed the energy conservation during the propagation steps, by preserving the absolute value of the particle’s velocity vector.

The integration accuracy, represented by the accepted truncation error in the RK5 technique, has been optimized correlating the backtracked directions with the selected astrophysical objects. An accuracy level of  $10^{-6}$  has been adopted, for which the changes in the backtracked directions become negligible with respect to the chosen step in angular separation  $d_{\text{max}}$  from the catalogue objects (see the section VI-A).

The cosmic ray trajectory has been followed till the galactocentric distance of 20 kpc (the Galaxy “border”), beyond which the field strength is supposed to be negligibly small.

## III. CONSIDERED LARGE-SCALE GMF MODELS

A strong large-scale magnetic field with a stationary or oscillating configuration can be generated from a weak seed field as a result of the non-uniform (differential) rotation of the galactic gas with strong turbulent motions [2]. The regular field structure obtained by this so-called dynamo mechanism can be described by modes of different azimuthal symmetry in the disk, and vertical symmetry perpendicular to the disk plane. The strongest mode is the spiral disk field with either  $\pi$  (*bisymmetric*, or BSS) or  $2\pi$  (*axisymmetric*, or ASS) symmetry. Other weaker field modes can also be excited. As for the vertical symmetry, the large-scale galactic fields can either keep the direction while traversing the disk plane (be of *even parity*), either change it to the opposite (*odd parity* modes). Both symmetry properties are reflected in the toponym of the large-scale field models. Combined with the spiral structure type, 4 possible spiral field patterns are denoted **BSS-S**, **BSS-A**, **ASS-S**, **ASS-A**, where -S (symmetric) stands for the even parity, and -A (antisymmetric) – for the odd parity.

We have chosen amongst many available large-scale GMF models three typical ones with distinct qualitative differences. Two models are the spiral disk field models of *bisymmetric even parity*, and *axisymmetric odd parity* from the paper [16] by Harari, Mollerach and Roulet (HMR). These models (see Fig. 1) represent a version of the Stanev model [15], smoothed out in order to avoid the field discontinuities.

The third model is a modification of the model [19] by Prouza and Šmída (PS), that has been proposed by Kachelrieß *et al.* [20]. In addition to the *bisymmetric even parity* spiral field, of the structure similar to the one in the HMR BSS-S model, it features two additional large-scale halo GMF components: *toroidal* azimuthal field above and below the Galactic disk, and *poloidal* (dipole) field.

## IV. PARAMETERS ADOPTED FOR SIMULATED CR EVENTS

We simulated a large number (stated in Tab. I and II) of cosmic ray events with the parameters below.

### A. Energy spectrum

The energy values of the simulated events were bounded between 40 EeV and 150 EeV, and distributed according to the Auger measurement [14], as a power law  $E^{-4.2}$ .

### B. Angular distribution

Two options for the angular distribution of the events have been considered: 1) Uniform distribution over the whole sky, and 2) Distribution according to the exposure of the Auger Surface Detector (SD) for zenith angles  $\theta_z \leq 60^\circ$ . For the considered energies the Auger SD acceptance area is saturated, which produces a simple analytic dependence of the exposure upon declination [27].

### C. Primary mass composition

4 pure compositions have been considered: protons ( $Z = 1$ ), carbon ( $Z = 6$ ), silicon ( $Z = 14$ ), and iron ( $Z = 26$ ) nuclei.

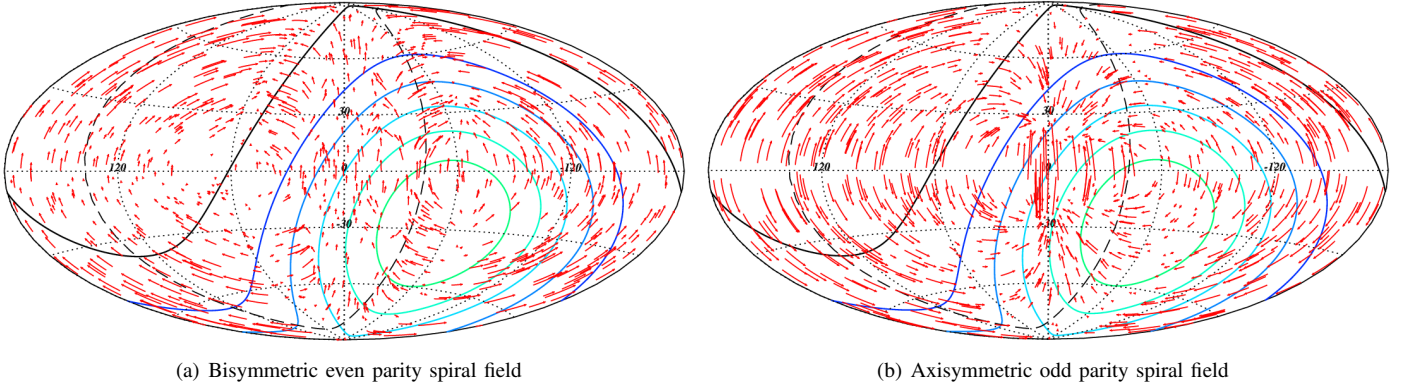


Fig. 2. Cosmic ray deflection patterns expected for *protons* under HMR models [16]. The deflections shown represent the arcs of the great circle joining the simulated arrival direction on Earth, and the backtracked one at the Galaxy border (indicated by an arrow head). To visualize deflections, every 100<sup>th</sup> event has been drawn from the large simulated event data sample described in the section IV. The dashed line denotes the supergalactic plane. The thin solid lines show the equal integrated Auger SD exposure sky regions within the detector field of view for zenith angles  $\theta_z \leq 60^\circ$ , delimited by the black solid line.

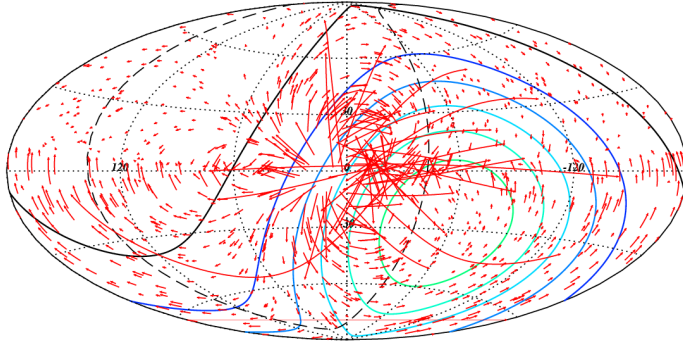


Fig. 3. *Idem* as Fig. 2 for the PS model [19] version by Kachelrieß *et al.* [20].

## V. MAGNETIC DEFLECTIONS OF COSMIC RAYS

The cosmic ray deflection patterns expected from the three selected GMF models are very different, as it can be seen from Figs. 2 and 3 on the example of primary *protons*. Except for the directions towards the Galactic Center, where the character of deflections is complex due to the multiple field reversals, there are trends, typical for each model. In the bisymmetric even parity spiral disk field, there is a flow in the direction of the Galactic North Pole, i.e. cosmic rays in general arrive at the Galactic halo border from higher Galactic latitudes than observed on Earth. In the odd parity field, the backtracked arrival directions in each Galactic hemisphere are shifted to the poles. This field configuration would obscure the Earth sky from the cosmic rays coming from the directions close to the Galactic plane. The presence of dipole and toroidal fields makes the deflection pattern even more complex (see Fig. 3).

The cumulative distributions (c.d.f.) of resulting deflections for the HMR BSS\_S model are shown on Fig. 4. The deflection values for the three considered GMF models are summarized in the table I, by means of percentiles at 50% (median), 68.27%, and 95.45% of the c.d.f. Neglecting the distribution tails, one can see that the deflection values scale rather well with the atomic number  $Z$  of primary nuclei. Despite the

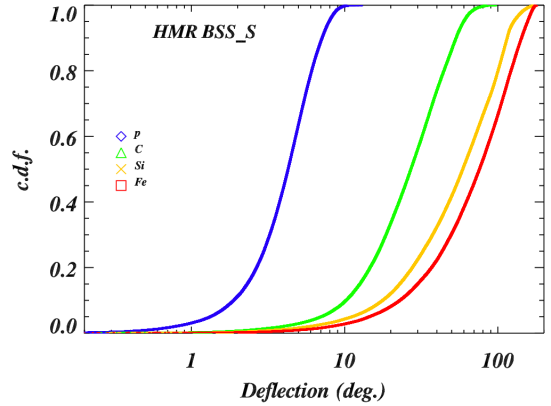


Fig. 4. C.d.f. of the deflection angle values (in  $^\circ$ ), expected in the HMR BSS\_S model [16] for the four assumed mass compositions.

Primary	Z	Uniform $4\pi$ exposure:			
		$N_{events}$	$\vartheta_{50\%}$	$\vartheta_{68.27\%}$	$\vartheta_{95.45\%}$
<b>HMR bisymmetric even parity model</b>					
p	1	100000	4.3	5.3	8.0
C	6	100000	27.1	36.5	60.7
Si	14	100000	59.1	82.6	129.1
Fe	26	100000	75.9	102.7	157.7
<b>HMR axisymmetric odd parity model</b>					
p	1	100000	5.4	6.6	10.9
C	6	100000	31.5	40.2	77.9
Si	14	100000	75.9	97.6	139.2
Fe	26	100000	84.0	100.4	138.0
<b>PS model version by Kachelrieß <i>et al.</i></b>					
p	1	20000	3.0	4.3	20.8
C	6	20000	16.7	22.9	64.7
Si	14	20000	37.6	47.2	85.7
Fe	26	20000	57.5	70.9	118.5

TABLE I

MAGNETIC DEFLECTIONS (IN  $^\circ$ ) AT THE INDICATED PERCENTILES OF THE C.D.F. (SHOWN ON FIG 4 FOR ONE OF THE THREE GMF MODELS).

additional halo fields in the PS model version, the higher overall normalization of the disk field strength in the HMR models, and its more important halo extension [16], [19], [20] are the reasons why in average the deflections for the HMR models are larger.

It is instructive to compare the obtained UHECR deflections (see Fig. 4) with those expected for turbulent field with a coherence length  $l_{\text{coh}}$ . In such a case, on a distance  $d \gg l_{\text{coh}}$  a cosmic ray will propagate in the random walk regime, with the resulting r.m.s. deflection angle given by [22], [23]

$$\vartheta_{\text{random}} [^\circ] \sim 1.13^\circ Z \frac{\sqrt{d [\text{kpc}]} \sqrt{l_{\text{coh}} [100 \text{ pc}]} B [\mu\text{G}]}{E [10 \text{ EeV}]}, \quad (2)$$

where the effect of dynamical friction [22] is taken into account. The path  $d$  can be roughly estimated using the simulated events (see Sec. IV). For the HMR BSS\_S field configuration, the median distance  $d_{50\%}$  traveled till the Galaxy border is 21.0 kpc for protons, and 28.3 kpc for iron nuclei, while the respective values for the two primaries corresponding to 95.45% of the c.d.f. are 28.1 kpc and 70.3 kpc. Under reasonable assumption of the equal field strength for the large-scale and turbulent components, an r.m.s. turbulent field strength is expected to decrease with a distance to the Galactic plane at a kiloparsec scale, which is much smaller than the above mentioned  $d$  values. Hence, for the energies of interest and for most of the directions in the sky the UHECR deflections from the random Galactic field component (2) will be considerably smaller than the ones from the large-scale GMF (see also [28]). Therefore, the former can be neglected at the first approach, though a realistic simulation of the UHECR propagation in the Galactic magnetic field has to take into account the turbulent field.

## VI. GMF EFFECTS ON THE EXTRAGALACTIC EXPOSURE

In addition to magnetic deflections, (de-)focusing effects of the Galactic magnetic field will modify the exposure of an experiment to the extragalactic sky [16], [17], [20]. Though the Liouville theorem holds and the isotropic cosmic ray flux outside the Galactic halo will remain isotropic on Earth, the correspondence between the arrival directions on Earth, and the sources contributing to the flux on the halo border will be quite complex. To study how this correspondence is realized, we have used the backtracked simulated events from the section IV. We mapped the decimal logarithm of the ratio of the number of events on the halo border ( $r = 20$  kpc) to the one on Earth, using the HEALPix equal area celestial sphere pixelization [29]. These maps, shown on Figures 5, 6, and 7 allow to estimate the (de-)magnification effects of the large-scale field on the experimental exposure.

Due to these effects, some regions of the sky have increased probability to contribute to the cosmic rays observed on Earth, and some other are disfavored. The non-uniform character of the mapping strengthens in the case of the heavy primary composition. There exist directions, for which the Earth detectors are blind, i.e. even if there is a strong UHECR source in such

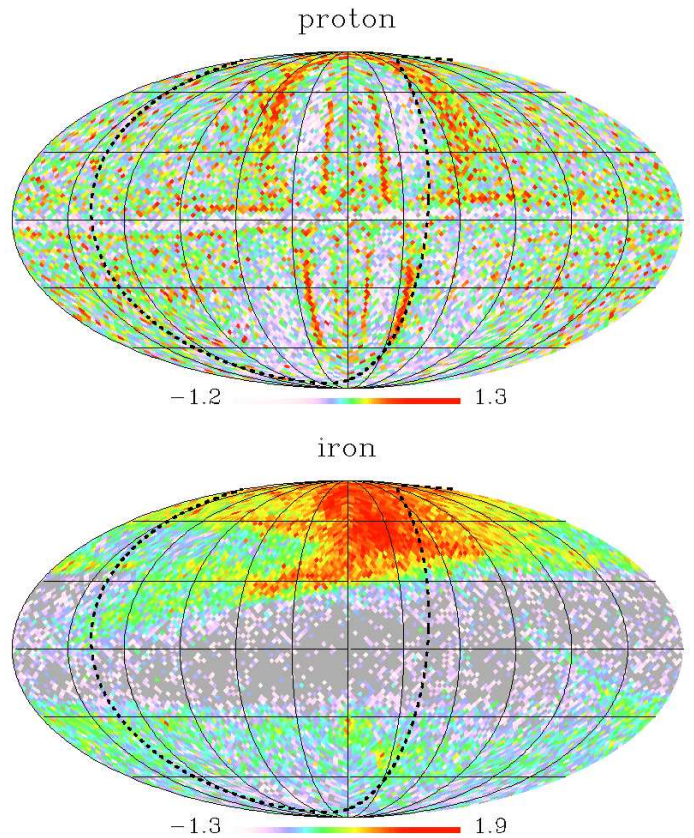


Fig. 5. The sky distribution of the  $\log_{10}$  of the ratio of the number of events at the Galaxy border to the one on Earth, for the HMR *bisymmetric even parity* model [16]. The gray color represents the regions on the sky, to which the Earth detectors are (almost) blind, like the one towards the Galactic Center on the lower plot. The arrival direction distribution on Earth is isotropic. The assumed cosmic ray primary type is indicated above each map. The thick dashed line denotes the supergalactic plane.

a “discriminated” sky region, heavy nuclei from this source will not reach the Earth. The highly non-uniform mapping in the case of pure iron primary composition is demonstrated by the lower plots on Figs. 5, 6, and 7. If the primary cosmic rays above 40 EeV are iron nuclei, and the GMF structure is adequately described by one of the assumed large-scale GMF models, the regions that would effectively contribute to the cosmic ray flux on Earth represent only a small fraction of the  $4\pi$  solid angle.

### A. Correlation scan using backtracked directions

To quantify these large-scale GMF effects on the mapping between the arrival directions on Earth and those at the Galaxy border in the case of the Pierre Auger Observatory, we performed a correlation analysis using *backtracked* arrival directions of simulated events described in Sec. IV, and the 694 AGN at redshift  $z_{\text{max}} \leq 0.024$  from the VCV catalogue. The simulated events have been divided sequentially into samples with the same number of events (81) above 40 EeV as in the Auger data. The employed set and ranges of parameters were also identical to the ones from [11], [12]. The lower

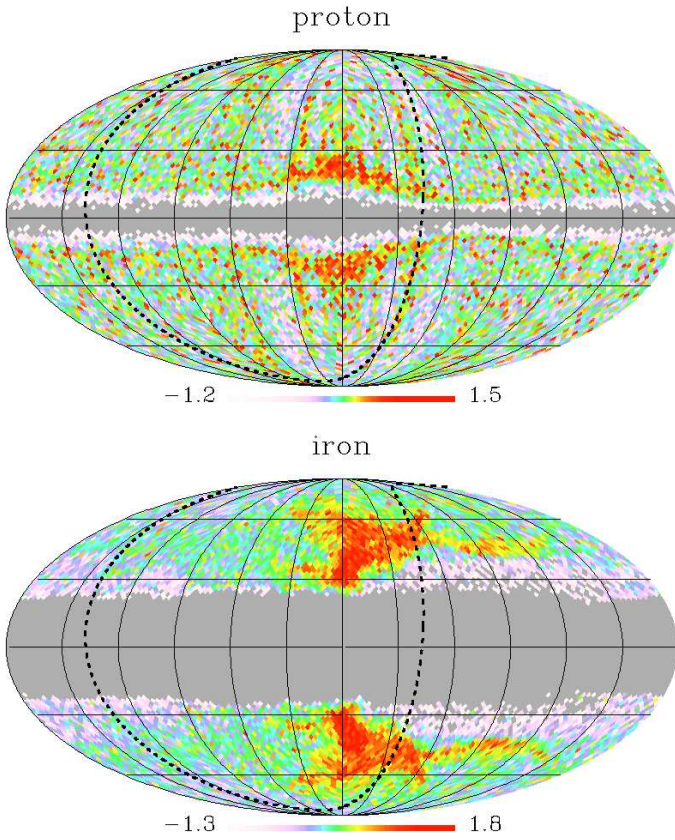


Fig. 6. *Idem* as Fig. 5 for the HMR axisymmetric odd parity model [16].

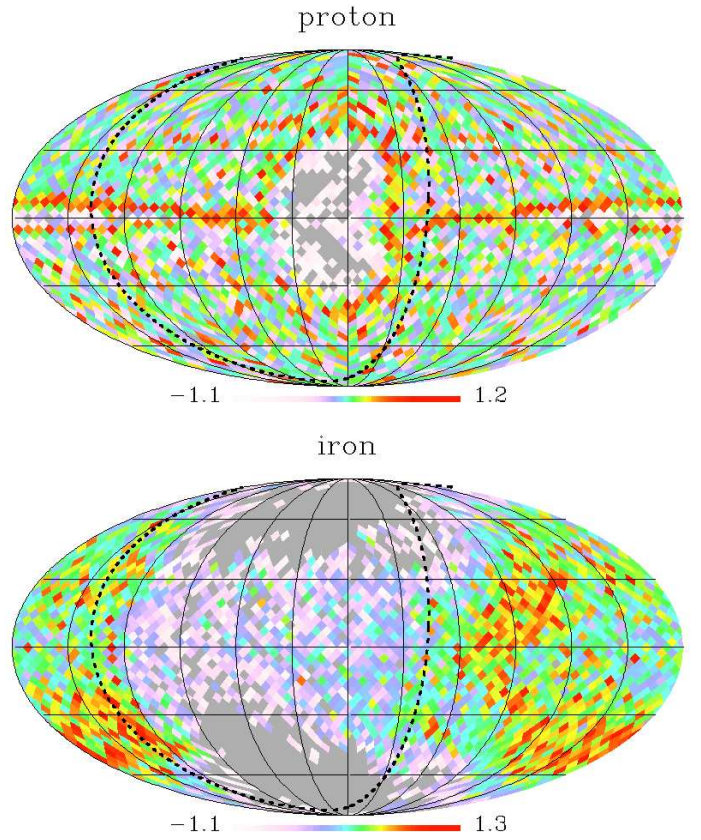


Fig. 7. *Idem* as Fig. 5 for the PS model [19] version by Kachelrieß *et al.* [20].

threshold energy giving maximal correlation was scanned within a range  $E_{\min} \geq 40 \text{ EeV}$ . The maximum redshift  $z_{\max}$  scan was performed within a range  $0 \leq z_{\max} \leq 0.024$ , in steps of 0.001. The scan in maximum angular distance  $d_{\max}$  was made within a range  $1^\circ \leq d_{\max} \leq 8^\circ$ , in steps of  $0.1^\circ$ .

We will focus here on the minimum probability values, obtained during the scan. The c.d.f. of decimal logarithm of the corresponding cumulative binomial probability  $P_{\min}$  of reaching this level of correlation under isotropy for the HMR BSS\_S model are shown on Fig. 8. The level of the minimum probability reached in the Auger data is also indicated. The results of the correlation scan for the three assumed large-scale GMF models and four primary mass compositions are summarized in Table II.

Since for the different GMF model/primary mass assumptions the backtracked directions correlate with the catalogue objects in particular privileged regions in the sky, our scan results depend strongly on those assumptions. Under some configurations, the backtracked directions lie near the supergalactic plane, where the catalog object density is higher than in average, which increases the correlation probability. For the PS model [19] version by Kachelrieß *et al.* [20], the scanned probability minimum is significantly less deep than for the two other spiral-field-only models for any assumed primary mass composition, except for protons, where one obtains nearly

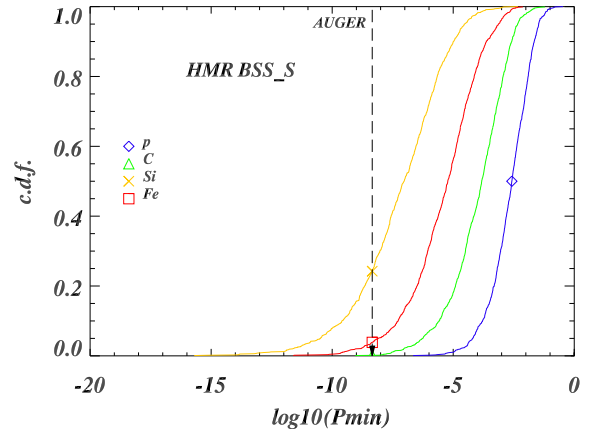


Fig. 8. Scan results for the simulated event samples, backtracked under the HMR bisymmetric even type model [16]. The four cumulative distributions of  $\log_{10} P_{\min}$  correspond to primary assumptions of pure protons, carbon, silicon, or iron nuclei. The vertical dashed line indicates the value obtained from the scan of the Auger events [11], [12] on Earth.

the same level of correlation for all models. The model with additional halo field components is clearly less compatible with the observed correlation with the nearby AGN [11], [12], unless the UHECR flux contribution from these objects (or objects with similar spatial distribution) is highly non-uniform

Primary	Auger SD exposure:				
	Z	$N_{samples}^{8l\ event}$	$f_{5\%}$	$f_{50\%}$	$f_{95\%}$
<b>HMR bisymmetric even parity model</b>					
p	1	1148	-4.20	-2.58	-1.47
C	6	1148	-6.26	-3.82	-2.34
Si	14	1147	-10.49	-7.03	-4.53
Fe	26	1148	-8.10	-5.22	-3.13
<b>HMR axisymmetric odd parity model</b>					
p	1	1148	-4.48	-2.70	-1.57
C	6	1148	-8.69	-5.78	-3.70
Si	14	1148	-12.56	-8.50	-5.30
Fe	26	1148	-8.98	-5.89	-3.85
<b>PS model version by Kachelrieß <i>et al.</i></b>					
p	1	308	-4.46	-2.66	-1.45
C	6	308	-4.55	-2.55	-1.43
Si	14	308	-5.21	-2.92	-1.72
Fe	26	308	-4.46	-2.52	-1.31

TABLE II

VALUES OF  $\log_{10} P_{\text{MIN}}$  AT THE INDICATED PERCENTILES OF THE C.D.F.,  
FOR THE ASSUMED GMF MODELS AND PRIMARY COMPOSITIONS.

(for example, if there are only few powerful sources, one of which is located by chance in one of those regions in the sky, where the large-scale field “enhances” the Auger exposure).

The presented approach has therefore a potential of providing constraints that can be used to discriminate between the GMF models and/or the primary charge. It is now being complemented by a forward-tracking of cosmic rays to the Earth, for a number of plausible UHECR sources scenarios.

## VII. CONCLUSIONS

We have studied the propagation of highest energy cosmic rays in the Galactic magnetic field, for different assumptions on the large-scale field structure and/or primary cosmic ray mass composition. The knowledge of the field distribution in the Milky Way is limited by the sensitivity and angular resolution of the present-day instruments. The Pierre Auger Observatory data provide the measurements of the primary cosmic ray properties with unprecedented level of collected statistics and reconstruction accuracy. This allows a complementary and independent way of probing the Galactic field structure. The observed correlation between the highest energy Auger events and the nearby AGN may give additional hints about the GMF amplitude and orientation.

We have investigated deflection patterns of cosmic rays above 40 EeV, underwent during their propagation in the Galactic field under three distinctively different GMF models. The exact deflection value in the regular component of the field depends strongly on the arrival direction on Earth of a cosmic ray, with the corresponding position angle of deflection differing from one assumed field distribution to another. In addition, the spectrometric character of deflections of the UHECR in the large-scale Galactic magnetic field gives rise to the aligned structures of events coming from a UHECR source (thread-like multiplets), that can be used

to discriminate between GMF models (see [30] and the references therein).

Magnetic deflections and (de-)focusing effects of the Galactic magnetic field modify the exposure of an experiment to the extragalactic sky. Our studies show that the UHECR picture observed on Earth is sensitive to the Galactic field distribution and the primary cosmic ray composition. Though the reconstruction of the field is easier in the case of light primary mass composition, in the case of heavy nuclei the lensing effects of the Galactic field on the exposure bring stronger constraints on the list of potential UHECR source candidates. The presented analysis of the correspondence between the arrival direction distributions on Earth and at the Galactic border, and of matching of the latter with the VCV catalogue objects will be complemented by the forward-tracking of cosmic rays for a number of plausible UHECR sources scenarios. This will allow for direct comparison with the observed AGN correlation.

## ACKNOWLEDGEMENTS

We acknowledge the discussions and cross-checks of results with E. M. Santos at the initial stage of the presented work.

## REFERENCES

- [1] R. Beck, Space Sci. Rev., **99** (2001) 243, astro-ph/0012402.
- [2] L. M. Widrow, Rev. Modern Phys. **74** (2002) 775, astro-ph/0207240.
- [3] J. E. Everett *et al.*, Astrophys. J. **674** (2008) 258, arXiv:0710.3712.
- [4] D. Breitschwerdt, Nature **452** (2008) 826.
- [5] J. L. Han *et al.*, Astrophys. J. **642** (2006) 868, astro-ph/0601357.
- [6] J. C. Brown *et al.*, Astrophys. J. **663** (2007) 258, arXiv:0704.0458.
- [7] H. Men, K. Ferrière, J.L.Han, Astron. & Astrophys. **486** (2008) 819, arXiv:0805.3454.
- [8] <http://www.lofar.org>
- [9] R. Beck, Adv. Radio Science, **5** (2007) 399.
- [10] <http://www.auger.org>
- [11] J. Abraham *et al.* [Pierre Auger Collaboration], Science **318** (2007) 939, arXiv:0711.2256.
- [12] J. Abraham *et al.* [Pierre Auger Collaboration], APh **29** (2008) 188, arXiv:0712.2843.
- [13] M.-P. Véron, P. Véron, Astron. & Astrophys. **455** (2006) 773.
- [14] J. Abraham *et al.* [Pierre Auger Collaboration], PRL 101 (2008) 061101, arXiv:0806.4302.
- [15] T. Stanev, Astrophys. J. **479** (1997) 290, astro-ph/9607086.
- [16] D. Harari, S. Mollerach, and E. Roulet, JHEP **08** (1999) 022, astro-ph/9906309.
- [17] J. Alvarez-Muñiz, R. Engel, and T. Stanev, ApJ **572** (2002) 185, astro-ph/0112227.
- [18] P. G. Tinyakov and I. I. Tkachev, APh **18** (2002) 165, astro-ph/0111305.
- [19] M. Prouza and R. Šmída, Astron. & Astrophys. **410** (2003) 1, astro-ph/0307165.
- [20] M. Kachelrieß, P.D. Serpico, and M. Teshima, APh **26** (2007) 378, astro-ph/0510444.
- [21] H. Takami, K. Sato, The Astrophysical Journal, **681** (2008) 1279, arXiv:0711.2386.
- [22] A. Achterberg *et al.*, 1999, astro-ph/9907060.
- [23] P. Bhattacharjee and G. Sigl, Phys. Rep. **327** (2000) 109, astro-ph/9811011.
- [24] J. W. Cronin, Nucl. Phys. B (Proc. Suppl.) **138** (2005) 465, astro-ph/0402487.
- [25] W. H. Press *et al.*, *Numerical Recipes in C. The Art of Scientific Computing*, Cambridge University Press, 2002, ISBN 0-521-43108-5.
- [26] E. Armengaud, PhD Thesis (in French), Université Paris 7 (2006), <http://apcauger.in2p3.fr/Public/Theses/Armengaud.pdf>
- [27] P. Sommers, Astropart. Phys. **14** (2001) 271, astro-ph/0004016.
- [28] P. G. Tinyakov and I. I. Tkachev, APh **24** (2005) 32, astro-ph/0411669.

- [29] K. M. Górski *et al.*, *Astrophys. J.* **622** (2005) 759, astro-ph/0409513.
- [30] D. Harari, S. Mollerach, and E. Roulet, *JHEP* **0207** (2002) 006, astro-ph/0205484.